AGU PUBLICATIONS

Geochemistry, Geophysics, Geosystems

RESEARCH ARTICLE
10.1002/2014GC005530

Changing tectonic controls on the long-term carbon cycle from Mesozoic to present

Benjamin Mills[1], Stuart J. Daines[1], and Timothy M. Lenton[1]

[1]College of Life and Environmental Sciences, University of Exeter, Exeter, UK

Key Points:
- We construct a forward model of granite, basalt, and seafloor weathering
- High Mesozoic CO_2 degassing countered by basalt and seafloor weathering
- Three distinct weathering regimes identified during 230 Ma to present

Supporting Information:
- LIP table
- BA_forcing_data
- Supporting information

Correspondence to:
B. Mills,
b.j.w.mills@exeter.ac.uk

Citation:
Mills, B., S. J. Daines, and T. M. Lenton (2014), Changing tectonic controls on the long-term carbon cycle from Mesozoic to present, *Geochem. Geophys. Geosyst.*, *15*, 4866–4884, doi:10.1002/2014GC005530.

Received 30 JUL 2014
Accepted 6 NOV 2014
Accepted article online 11 NOV 2014
Published online 17 DEC 2014

Abstract Tectonic drivers of degassing and weathering processes are key long-term controls on atmospheric CO_2. However, there is considerable debate over the changing relative importance of different carbon sources and sinks. Existing geochemical models have tended to rely on indirect methods to derive tectonic drivers, such as inversion of the seawater $^{87}Sr/^{86}Sr$ curve to estimate uplift or continental basalt area. Here we use improving geologic data to update the representation of tectonic drivers in the COPSE biogeochemical model. The resulting model distinguishes CO_2 sinks from terrestrial granite weathering, total basalt weathering, and seafloor alteration. It also distinguishes CO_2 sources from subduction zone metamorphism and from igneous intrusions. We reconstruct terrestrial basaltic area from data on the extent of large igneous provinces and use their volume to estimate their contribution to degassing. We adopt a recently published reconstruction of subduction-related degassing, and relate seafloor weathering to ocean crust creation rate. Revised degassing alone tends to produce unrealistically high CO_2, but this is counteracted by the inclusion of seafloor alteration and global basalt weathering, producing a good overall fit to Mesozoic-Cenozoic proxy CO_2 estimates and a good fit to $^{87}Sr/^{86}Sr$ data. The model predicts that seafloor alteration and terrestrial weathering made similar contributions to CO_2 removal through the Triassic and Jurassic, after which terrestrial weathering increased and seafloor weathering declined. We predict that basalts made a greater contribution to silicate weathering than granites through the Mesozoic, before the contribution of basalt weathering declined over the Cenozoic due to decreasing global basaltic area.

1. Introduction

Atmospheric CO_2 is thought to have fluctuated considerably over geologic time, with solar, biological and tectonic forcing factors all having an effect. Models of the long-term carbon cycle aim to capture these various drivers, alongside the key processes, in order to predict past changes in atmospheric CO_2 [*Arvidson et al*., 2006; *Bergman et al*., 2004; *Berner*, 1991, 2006a]. Model predictions can be tested against CO_2 proxy estimates [*Park and Royer*, 2011], which become more frequent toward the present day. During most of the Mesozoic and Cenozoic the climate has been warmer than today, with proxy estimates suggesting generally elevated atmospheric CO_2. Existing models suggest tectonic factors were a key driver of CO_2 fluctuations during this interval [*Berner*, 2006b; *Li and Elderfield*, 2013], with increased degassing input producing higher atmospheric CO_2 during the Mesozoic, and then a combination of declining degassing and increasing weatherability of the land surface (due in particular to mountain building [*Raymo and Ruddiman*, 1992]) causing CO_2 to decline during the Cenozoic. However, the pattern and magnitude of variation in tectonic forcing factors is uncertain, and correspondingly there is considerable disagreement over the varying contribution of different CO_2 source and sink processes over Mesozoic-Cenozoic time.

Existing models generally use indirect methods to estimate variations in tectonic forcing factors such as degassing rates and the supply of easily weathered volcanic rocks [*Berner*, 2006b]. However, recent advances now make it possible to estimate these variations in forcing more directly from geological and geophysical data. Notably, *Van Der Meer et al*. [2014] have produced a reconstruction of combined arc and ridge CO_2 degassing over the last 230 million years based on the length of subduction zones reconstructed from geophysical "imaging" of subducted plates. Compared to earlier work, the result is markedly increased degassing through much of the Mesozoic. The authors use their new degassing function to force a version of the GEOCARBSULF geochemical model [*Berner*, 2006a]. They find that bringing CO_2 predictions back into agreement with proxy data for the Mesozoic is possible but requires an enhancement of the CO_2 sink via silicate weathering, which is achieved by tuning a parameter that represents the contribution of continental basalt

weathering [*Berner*, 2006b], such that it is at its maximum permissible value. However, the contribution of basalts to continental weathering is also amenable to more direct estimation from geologic data regarding the timing and extent of large igneous provinces and the rate of material subduction driving island arc basalt production.

Motivated by this, here we revisit how tectonic drivers of the long-term carbon cycle have changed over Mesozoic and Cenozoic time. We seek to build an internally consistent forward model, by updating the tectonic forcing factors in our existing "COPSE" biogeochemical model [*Bergman et al*., 2004] and elaborating the different weathering sinks for CO_2 from granites, basalts, and seafloor alteration—a carbon sequestration process that has been incorporated into models for Precambrian climate [*Sleep and Zahnle*, 2001; *Hayes and Waldbauer*, 2006] but has not been assessed fully over the Phanerozoic. We reconstruct terrestrial basaltic area from data on the extent of large igneous provinces and plate subduction rates, and use LIP volume to estimate their contribution to degassing. We also adopt the new reconstruction of degassing by *Van Der Meer et al*. [2014] and revise the uplift forcing in the model (so that it is independent of the strontium isotope record, which the model now seeks to predict). We address whether the resulting model of changes in atmospheric CO_2 is in broad agreement with proxy data for both the *Van Der Meer et al*. [2014] and original GEOCARB degassing scenarios, examine which processes most likely acted to counter the high CO_2 degassing rates reported in the former, and how the contribution of each CO_2 sink has changed over the Mesozoic and Cenozoic.

2. Tectonic Controls on the Long-Term Carbon Cycle

The inorganic side of the long-term carbon cycle involves a balance between degassing sources of CO_2 from volcanic and metamorphic processes and weathering sinks of CO_2, which involve the liberation of Ca^{2+} and Mg^{2+} ions from silicate rocks and their deposition in carbonate rocks along with oceanic CO_3^{2-}. These sources and sinks of CO_2 are affected by changes in tectonic processes, which hence can exert a major control on atmospheric CO_2 concentrations over geologic time.

Key long-term sources of CO_2 are metamorphic degassing from carbonates (and organic matter) and direct injection of CO_2 from the mantle. Metamorphic degassing is driven by subduction of oceanic crust at continental margins, and input of mantle CO_2 is associated with crustal production at mid-ocean ridges and with the emplacement of large igneous provinces. LIP emplacement in continental settings also results in contact metamorphism of carbon reservoirs in the adjacent crust [*Svensen et al*., 2009].

The long-term sinks of CO_2 involve the weathering of subaerial granites and basalts [*Dessert et al*., 2003], and the carbonatization of seafloor basalts [*Gillis and Coogan*, 2011]. Uplift of the continents provides a fresh supply of (primarily granitic) material for terrestrial silicate weathering. Subduction-driven arc volcanism and the emplacement of continental LIPs provide basaltic material, which undergoes more rapid silicate weathering. Additionally, seafloor spreading provides a fresh supply of basaltic ocean floor for seafloor carbonatization/alteration, which occurs when warm seawater flows through the crust.

2.1. Degassing: Metamorphism, Ridge, and LIPs

We show in Figure 1 a comparison between the recent calculation of global degassing rate based on scaling combined arc and ridge CO_2 degassing to inferred subduction zone length [*Van Der Meer et al*., 2014] and that previously employed in carbon cycle models, which is based on inversion of paleo-sea level records [*Gaffin*, 1987] prior to 150 Ma and measurements of trench convergence [*Engbretson et al*., 1992] since 150 Ma to estimate global spreading rate.

In addition, eruption of large igneous provinces is accompanied by massive CO_2 input over a geologically short time scale ($<10^6$ years). If input was sufficiently rapid, geochemical box models have predicted very large CO_2 increases (e.g., around a doubling of pre-LIP atmospheric CO_2 concentration for the Siberian traps and Central Atlantic Magmatic Province (CAMP) emplacements, assuming input times between 30 and 500 kyr [*Beerling and Berner*, 2002; *Berner*, 2002]). Stabilization of climate occurs in these models after $\sim$2 Myr, but the background forcing scenarios we will consider (i.e., altered degassing rates, weathering regimes, and burial rates) and large weatherable area of some of the LIPs may affect both peak CO_2 concentrations and stabilization times. Shorter term effects such as contact metamorphism of organic sediments and

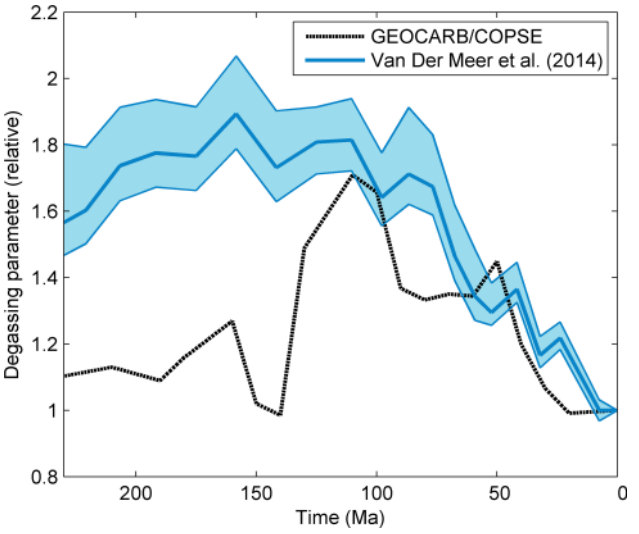

Figure 1. Global CO_2 degassing. Black line shows relative CO_2 degassing rate assumed in previous models GEOCARB [*Berner*, 2006a] and COPSE [*Bergman et al.*, 2004], among others. Blue shaded area shows recently calculated degassing parameter taking into account subduction zone length [*Van Der Meer et al.*, 2014].

methane release [*Svensen et al.*, 2009] may have led to larger increases in CO_2 and global temperatures following LIP emplacements [*Belcher and Mander*, 2012].

2.2. Silicate Weathering: Granites and Basalts

Dependency of silicate weathering rates on local temperature and runoff allows the carbon burial flux from silicate weathering and carbonate deposition to vary in response to changes in atmospheric CO_2, resulting in negative feedback which balances the long term carbon cycle [*Walker et al.*, 1981]. As well as changes in temperature, there are many other factors that influence the long term global silicate weathering rate and resulting marine carbonate burial flux. Enhancements of the weathering flux may be brought about by increases in global erosion rates [*Dixon et al.*, 2012] (which may lead to changes in climate dependence of weathering [*West*, 2012]), the presence of land plants (which introduce organic acids as well as physically breaking apart rock) [*Berner*, 1997], or changes in the hydrological cycle [*Maher and Chamberlain*, 2014] including the paleolatitude and relative positioning of the continents [*Goddéris et al.*, 2014]. Altering these factors changes the global terrestrial "weatherability"—the total silicate weathering rate under a given CO_2 concentration. A higher weatherability means that the carbon cycle will stabilize with a lower concentration of atmospheric CO_2, providing the CO_2 degassing rate is unchanged [*Kump and Arthur*, 1997]. Essentially, the long term stable concentration of CO_2 is determined by a combination of the global degassing rate and the weatherability of terrestrial silicates (and the ocean floor).

An important factor that influences terrestrial weatherability is the type and area of silicate rock available for weathering. Mafic silicates like basalt weather considerably more rapidly than felsic granites; less than 10% of the global silicate area is basaltic yet this contributes around one third of the silicate weathering flux today [*Dessert et al.*, 2003]. This means that changes in past global basaltic area may have led to significant changes in terrestrial weatherability, and therefore atmospheric CO_2 concentration.

2.3. Reconstructing Basalt Weathering

Current reconstructions of volcanic rock weathering (Figure 2) are produced by inversion of the marine $^{87}Sr/^{86}Sr$ and $^{187}Os/^{188}Os$ signatures [*Berner*, 2006b; *Li and Elderfield*, 2013]. The predominant sources of ocean Sr and Os are the weathering of terrestrial rocks, and there are no fractionation effects associated with weathering and burial of these species. This means that the seawater value, as recorded in sediments, reflects the contribution from different weathering sources and mantle inputs. $^{87}Sr/^{86}Sr$ and $^{187}Os/^{188}Os$ of fresh basalt reflects the value of the mantle source rocks, and decay of ^{87}Rb and ^{187}Re, respectively, causes the $^{87}Sr/^{86}Sr$ and $^{187}Os/^{188}Os$ of older granitic lithologies to be higher than the mantle value.

Berner [2006b] sets $^{87}Sr/^{86}Sr$ values for bulk volcanic and nonvolcanic silicates to obtain an expression linking the Phanerozoic seawater $^{87}Sr/^{86}Sr$ curve to the fraction of silicate weathering that was from volcanic sources (denoted X_{volc}). *Li and Elderfield* [2013] model the coupled Sr, Os, and C isotope systems to reconstruct long term carbon cycle fluxes from weathering and burial over the Late Cretaceous and Cenozoic. Both studies suggest a decreasing trend in basalt weathering over most of the Cenozoic. *Li and Elderfield* [2013] propose that weathering of (island) basalts has decreased in response to an uplift-driven increase in weathering of continental nonbasalt silicates.

However, there are several difficulties in using radiogenic isotope tracers to reconstruct terrestrial weathering regimes. The $^{87}Sr/^{86}Sr$ of nonvolcanic silicates [*Berner*, 2006b] and sedimentary carbonates [*Boucot and*

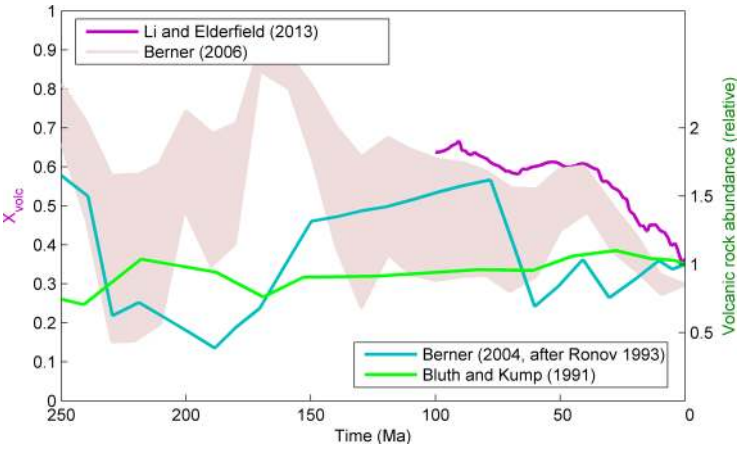

Figure 2. Reconstructions of volcanic weathering. X_{volc} (left axis) is the fraction of terrestrial silicate weathering that is volcanic (note that this includes contribution from island and arc basalts, which are included under "terrestrial silicates" in our analyses), calculated from inversion of the $^{87}Sr/^{86}Sr$ and $^{187}Os/^{188}Os$ curves [*Berner*, 2006b; *Li and Elderfield*, 2013]. Plotted here against relative abundance of volcanic rocks (right axis) [*Berner*, 2004; *Bluth and Kump*, 1991; *Ronov*, 1993].

Gray, 2001] varies greatly due to age and composition of weathered material, ruling out a straightforward link between ocean $^{87}Sr/^{86}Sr$ and fraction of volcanic weathering. Uncertainty in total rates of terrestrial weathering, mantle input and seafloor alteration also make the $^{87}Sr/^{86}Sr$ signal difficult to link directly to the volcanic fraction of weathering. Interpretation of the marine $^{187}Os/^{188}Os$ record is no less straightforward: preferential weathering of ancient shield rocks may result in a very radiogenic signal [*Peucker-Ehrenbrink and Blum*, 1998], similarly the weathering of more ancient basalts may impart a significantly more radiogenic signal than their younger counterparts [*Gannoun et al*., 2006]. Additional Os isotope variation may be associated with spatial heterogeneity in seawater, or by extraterrestrial Os sources such as impact events [*Peucker-Ehrenbrink and Ravizza*, 2012].

The Sr-derived curves for basalt weathering fraction have a large uncertainty due to the range of possible values for nonvolcanogenic Sr [*Berner*, 2006b], although predicted values for the Mesozoic are generally higher than the present day, and a decline in volcanic weathering over the Cenozoic is robustly predicted, due to continually rising $^{87}Sr/^{86}Sr$ ratios. Volcanic weathering reconstructions for the last 100 Myr using constraints from both Sr and Os isotopes [*Li and Elderfield*, 2013] show a general decline from 100 Ma to present.

Attempts have also been made to reconstruct the relative exposure of volcanics from rock abundance data. Using the historic volcanic rock volumes of *Ronov* [1993], *Berner* [2004] normalizes against an exponential loss curve to obtain an estimate of the rate of volcanic eruption over time. This shows above-present-day values for the Cretaceous, but lower-than-present values during the Triassic and Jurassic. However, this interpretation is not directly linked to the exposed area of volcanics to weathering, and the low values reported for$\sim$200 Ma are not easy to reconcile with eruption of the massive Central Atlantic Magmatic Province (CAMP) at this time—which is thought to have emplaced an area of basaltic rock of comparable size to the entire present-day volcanic area [*Knight et al*., 2004; *Marzoli*, 1999].

Bluth and Kump [1991] have produced historical land area for different rock units over the Phanerozoic. Assuming that the total area of silicates can be represented by total land area minus the area of carbonates, an expression for the fraction of exposed silicates that are of volcanic origin can be calculated [see *Berner*, 2006b]. The result is a slight increasing trend from the early Triassic to the present day.

The area of volcanics exposed to weathering during the Mesozoic is therefore very uncertain, with isotope-derived methods generally predicting areas in excess of the present day while rock abundance methods predict values that are lower. Interpretation of rock abundance data is however extremely difficult—normalizing via a single decay curve [*Berner*, 2004] or by noncarbonate area [*Berner*, 2006b] necessarily represent generalized preliminary approaches.

2.4. Seafloor Weathering

Low temperature hydrothermal alteration of mid-ocean ridge basalts (or "seafloor weathering") is a significant long-term carbon sink. If the oceanic crust provides the alkalinity source (via Ca^{2+} release), rather than riverine input (as Ca, or via Mg or K followed by cation exchange) [*Alt and Teagle*, 1999; *Coogan and Gillis*, 2013], then this operates independently from silicate weathering.

As with continental silicate weathering, it has been proposed that the rate of carbon uptake by the ocean crust is linked to atmospheric CO_2 concentration, resulting in negative feedback on climate. There is no clear direct link [*Caldeira*, 1995], but two indirect feedback mechanisms have been proposed. In the first, higher atmospheric CO_2 results in increased bottom water temperature, which increases rates of fluid-rock reaction [*Brady and Gislason*, 1997]. Second, potassium reacts with igneous plagioclase to form K-feldspar and liberate Ca from the oceanic crust (with stoichiometry 7 Ca^{2+}:2 K^{+}, i.e., the oceanic crust providing the majority of the alkalinity [*Coogan and Gillis*, 2013]). Therefore, increased atmospheric CO_2 should drive increased riverine K input (from continental weathering), ultimately resulting in enhanced seafloor weathering rates [*Coogan and Gillis*, 2013].

Drill core analysis has confirmed that more carbon is added to the ocean crust under warmer bottom water temperatures [*Gillis and Coogan*, 2011] and that high K-feldspar abundances are coincident with large fluxes of carbon into the ocean crust [*Coogan and Gillis*, 2013]. The majority of carbon added to the ocean crust is deposited within 20 Myr of crust formation [*Gillis and Coogan*, 2011], supporting the assumption that the rate of seafloor weathering is linked to the rate of ocean crust production at mid-ocean ridges through material availability [*Sleep and Zahnle*, 2001]. However, these feedback relationships are still very uncertain, and the strength of the feedback on CO_2 concentration is unknown. Recent studies investigating seafloor weathering [*Hayes and Waldbauer*, 2006; *Sleep and Zahnle*, 2001] assume a simple power law relationship between atmospheric CO_2 and the rate of carbon uptake, based on the laboratory results of *Brady and Gislason* [1997] for the bottom water temperature feedback. It is possible that the feedback may be substantially stronger or weaker than this.

The rate of seafloor weathering over the Phanerozoic is also unknown. A major complicating factor is that not all of the alkalinity deposited in ocean crust basalts has been weathered from the rock itself, it is possible that over 70% of the calcium may come from seawater [*Alt and Teagle*, 1999], meaning that much of the $CaCO_3$ deposited in the crust is linked instead to terrestrial weathering. However, the ocean crust alkalinity budget of *Coogan and Gillis* [2013] supports a major contribution from seafloor weathering. As indirect support, carbon abundances in the upper ocean crust [*Coogan and Gillis*, 2013; *Gillis and Coogan*, 2011] are substantially higher in the late Mesozoic than in the Cenozoic (up to five times higher wt. %), which is consistent with the hypothesis that higher material input from seafloor spreading [*Van Der Meer et al*., 2014] and atmospheric CO_2 concentrations [*Park and Royer*, 2011] drove increased seafloor weathering rates.

Berner and Kothavala [2001] add an expression for seafloor weathering to the "GEOCARB 3" model, linking the rate only to seafloor spreading rates, not to CO_2 concentration. Seafloor weathering does not contribute greatly to the carbon cycle in this model as the rate is assumed not to be affected by the high CO_2 concentrations, and the material supply from spreading centres is assumed to be low for much of the Mesozoic, in contrast to recent data [*Van Der Meer et al*., 2014]. Previous attempts to reproduce the Phanerozoic $^{87}Sr/^{86}Sr$ curve using a forward model rely on seafloor weathering being a more powerful carbon sink in the past, thus reducing the weathering contribution of the continents [*Francois and Walker*, 1992].

3. Methods

3.1. The COPSE Model

To analyze tectonic effects on climate we use an updated version of the COPSE model [*Bergman et al*., 2004]. For full model equations see supporting information, for discussion of the original model see the 2004 paper. COPSE is an extension of the GEOCARB [*Berner*, 1991, 2006a] models that employs a process-based representation of the marine and terrestrial biosphere [*Lenton and Watson*, 2000] to calculate organic fluxes of carbon and sulphur over Phanerozoic time. The philosophy behind COPSE is to use mechanistic approximations, rather than inversion of isotope records, to calculate geochemical fluxes. This parallels our approach here of reconstructing changes in weathering regimes from primary data rather than "weathering tracers" such as $^{87}Sr/^{86}Sr$ and $^{187}Os/^{188}Os$.

Changes in the global reservoir of atmospheric and ocean carbon (A) are represented by the following differential equation summing CO_2 sources from degassing of carbonates (*ccdeg*), organic material (*ocdeg*), LIP degassing (*LIPdeg*), carbonate weathering (*carbw*), and oxidative weathering of organics (*oxidw*). Sinks are the burial of organic carbon in the marine (*mocb*) and terrestrial (*locb*) environments, carbonate burial (*mccb*), and weathering/alteration of the seafloor (*sfw*)

$$\frac{dA}{dt} = ccdeg^{*} + ocdeg^{*} + oxidw + LIPdeg^{**} + carbw - mocb - locb - mccb - sfw^{**} \quad (1)$$

We calculate marine carbonate burial from steady state marine alkalinity balance, assuming the carbonate cycle is at equilibrium, and including the coupling of the oxidative sulphur cycle to alkalinity [*Torres et al*., 2014]:

$$mccb = silw + carbw - pyrw + mpsb \quad (2)$$

where *mpsb* is pyrite sulphur burial, and pyrw is pyrite sulphur weathering (in mol S yr^{-1}).

Substituting for *mccb* in (1) leads to the net equation:

$$\frac{dA}{dt} = ccdeg^{*} + ocdeg^{*} + oxidw + LIPdeg^{**} - mocb - locb - silw^{*} + (pyrw - mpsb) - sfw^{**}. \quad (3)$$

Here * refers to fluxes that are updated in this paper while ** shows fluxes that have been added to the model for this work.

The addition of sulfide oxidation and sulfate reduction in the carbon cycle [*Torres et al*., 2014] has little effect in our model, as steady state for the ocean alkalinity is assumed. A more complete ocean model is required to analyze the effects of possible transient CO_2 emissions in a global context.

3.2. Modeling CO_2 Input From Metamorphism and Degassing

Our first model runs will consider the metamorphism and ridge contribution of *Van Der Meer et al*. [2014], which is added to COPSE alongside an explicit representation of LIP CO_2 release. Relative global degassing rate, *D*, acts as a multiplier for the rates of degassing for organic (*ocdeg*) and carbonate carbon (*ccdeg*)

$$ocdeg = k_{ocdeg}\left(\frac{G}{G_0}\right) \times D \ , \quad (4)$$

$$ccdeg = k_{ccdeg}\left(\frac{C}{C_0}\right) \times D \times B, \quad (5)$$

where k_{ocdeg} and k_{ccdeg} are the present-day rates, *G*, *C* represent the total crustal inventory of organic carbon and carbonate carbon, respectively, and G_0, C_0 are their present-day sizes. *B* is the relative carbonate burial depth forcing, which is inherited from COPSE and GEOCARB, and represents the evolution of pelagic calcifiers which increases the amount of carbonate entering subduction zones.

We follow *Beerling and Berner* [2002] by scaling total LIP CO_2 release to the initial estimated basalt volumes. The timing, initial areas, and tectonic environment (terrestrial versus submarine) of large igneous provinces have been compiled by the Large Igneous Provinces Commission [*Ernst and Buchan*, 2001; *Ernst*, 2014] (Figures 3 and 4). We have updated this record where necessary (see supporting information and references therein). Where LIP volumes are unknown, we calculate them by assuming an area-volume relationship based on the more recent and well-preserved LIPs (see supporting information).

Figure 3 shows the volumes and CO_2 release potentials for all LIPs from 230 to 0 Ma. By far the largest volume event over the model timeframe is the ~125 Ma Ontong Java Plateau, with an estimated initial volume of around 5×10^7 km^3 [*Neal et al*., 1997]. This is 10 times the volume of the Siberian traps, which is itself one of the most voluminous LIPs on record. Cumulative CO_2 degassing from LIPs during the last 230 Ma is estimated here as 1–5 $\times$ 10^{19} moles. This represents around 1% of global cumulative CO_2 degassing over this period, but the geologically short time scale of these degassing events may lead to significant climate impacts.

For a maximum estimate of CO_2 emissions, we assume each LIP degasses over a time scale of 200 kyr [*Berner*, 2002] and assume the rate of degassing follows a Gaussian curve [*Beerling and Berner*, 2002]. Although 200 kyr is the "slow degassing" estimate from *Berner*'s work, more recent compilations suggest LIP degassing time scales are somewhat slower, in the range 500 kyr–3 Myr [*Courtilliot and Renne*, 2003]. We exclude here shorter term effects such as contact metamorphism of organic sediments and methane release [*Svensen et al*., 2009] as they are difficult to quantify and analyze with our long term model.

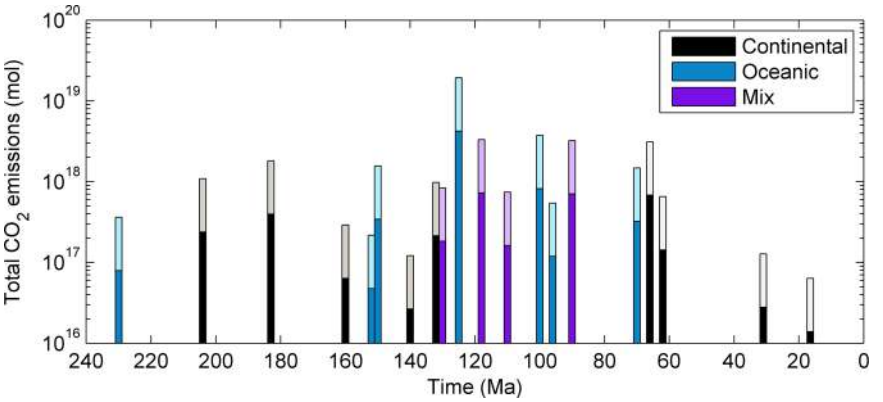

Figure 3. Submarine and continental LIP emplacement CO_2 emissions. Total moles of carbon degassed as CO_2 during LIP emplacement. Min and max estimates for CO_2 degassing/volume relationship are from *Leavitt* [1982] and *Gerlach and Graeber* [1985], respectively (following *Beerling and Berner* [2002]) and are denoted by darker and lighter colors, respectively.

3.3. Modeling Basalt and Granite Weathering

To obtain estimates for the weathering flux associated with basalts, we include the relative basalt area parameter as a time-dependant forcing in COPSE. The model calculates global silicate weathering rates using the expressions described in the GEOCARB models [*Berner*, 1994], and is modified here by splitting the silicate weathering term into "basalt," representing volcanics, and "granite," which represents all non-mafic terrestrial silicates:

$$basw = \%bas_0 \times k_{silw} \times f_{CO2bas} \times PG \times pevol \times BA, \tag{6}$$

$$granw = (1-\%bas_0) \times k_{silw} \times f_{CO2gran} \times PG \times pevol \times GA \times U, \tag{7}$$

$$silw = basw + granw. \tag{8}$$

Here *basw* and *granw* are the model fluxes for basalt weathering and granite weathering. *U* is normalized uplift rate, which is assumed to affect granites but not basalts, which are presumed to be continually well exposed. *PG* is the runoff modifier due to paleogeographic changes, the constant $\%bas_0$ is the present-day fraction of silicate weathering that is basaltic, chosen as 0.35 [*Dessert et al*., 2003] (granite weathering is assumed to make up the remainder of CO_2 consumption via terrestrial sillicate weathering), k_{silw} is the present-day rate of silicate weathering. *BA* is the relative basaltic area (calculated below and shown in Figure 5) and GA is the relative area of granites, which is calculated as the total silicate area minus that of continental basalts (see supporting information). *pevol* represents negative feedback on terrestrial weathering due to evolution of land plants, including fire feedback, photorespiration, and CO_2 fertilization as in the original COPSE model. See supporting information and the COPSE paper for full details of the vegetation model. f_{CO2bas} and $f_{CO2gran}$ denote the climatic dependency of silicate weathering [*Berner*, 1994], which incorporates plant-CO_2 feedbacks, and the temperature dependencies f_{Tbas} and f_{Tgran}, which assume activation energies for basalt and granite weathering of 42 and 50 kJ/mol, respectively [*Dupre et al*., 2003]

$$f_{Tbas} = e^{0.061(T-T_0)}\{1+0.038(T-T_0)\}^{0.65}, \tag{9}$$

$$f_{Tgran} = e^{0.072(T-T_0)}\{1+0.038(T-T_0)\}^{0.65}. \tag{10}$$

Here *T* is global average surface temperature and T_0 is present-day surface temperature.

The uplift/erosion forcing *U* is assumed to influence granite, carbonate and organic carbon (but not basalt) weathering fluxes via supply rate of material. In earlier versions of COPSE, values for *U* over the Phanerozoic are taken from the early GEOCARB models, and were calculated by inverting the strontium isotope record. We follow *Goddéris and Francois* [1995] and *Berner* [2006b] by replacing this with a cubic fit to sediment abundance data [*Ronov*, 1993] in order that no fluxes in the system depend on input of isotope tracer values. We also introduce the expression, *PG*, representing relative changes to global runoff due to changing paleogeography. *PG* is taken from published runs of the GEOCLIMtec model [*Goddéris et al*., 2014] and is assumed to affect all silicate and carbonate weathering fluxes.

Aside from the rock area (BA, GA) forcings, uplift rate, and activation energies, weathering of granites and basalts is assumed to follow the same dependencies. It is probable that factors such as plant cover, paleogeographic position and global runoff affect granite and basalt weathering in different ways. These effects are potentially important, but involve a high degree of uncertainty and require the use of a spatial model to accurately depict them [e.g., *Taylor et al*., 2012; *Lefebvre et al*., 2013]. Our modeling implicitly allows for the more rapid weathering of basalts via a simple scaling relationship (i.e., the assumption that doubling the area of exposed basalt will double the weathering flux from basalts).

3.4. Basaltic Area Reconstruction

We introduce a new method for calculating the past land area covered by basalts, which we reason must be a key driver of the rate of global basalt weathering. The present-day basaltic area is contributed by large igneous provinces, ocean island basalts, and island arcs. The total area has been estimated at 6.8×10^6 km^2 [*Dessert et al*., 2003]. Of this, 2×10^6 km^2 is contributed by ocean island basalt and island arcs [*Allègre et al*., 2010], with the remaining area related to existing large igneous provinces [*Dessert et al*., 2003]. In order to reconstruct total terrestrial basaltic area, we adopt an individual approach for each igneous emplacement.

Figure 4 shows the subaerial areas of LIPs emplaced during the Mesozoic and Cenozoic. The named events in the figure are those with areas $>10^6$ km^2, which contribute almost all of the total emplaced area, and which we term "major events." To construct the integrated LIP area exposed to subaerial weathering, we assume exponential decay curves for individual LIPs, representing removal by erosion. We set decay constants for each major event so that their present-day area is recovered (see supporting information for a list of these areas). We set a single decay constant that applies to all of the minor events, which is chosen so that present-day total LIP area is 4.8×10^6 km^2 [*Allègre et al*., 2010; *Dessert et al*., 2003]. This constant falls within the range applied to the major LIPs. Submarine LIPs are assumed not to influence terrestrial weathering rates, but do contribute to CO_2 release and may impact on seafloor weathering. Contributions to seafloor weathering from oceanic LIPs likely occur due to enhanced crustal production during emplacement [i.e., *Coffin and Eldholm*, 1994], and thus occur on a similar time scale to CO_2 degassing. We analyze LIP degassing and seafloor weathering enhancements together later in the paper (see Figure 8).

The approach of using exponential decay to account for erosional loss follows *Berner* [2004], but we apply it here to multiple individual events and to areas rather than volumes. We also trial an alternative approach where decay in area begins 10 Myr after emplacement, representing an assumed 10 Myr volcanic activity where basalt is being emplaced or replenished [*Bryan and Ernst*, 2008]. Of the present-day island arc and ocean island basalts, 87% of the total area is contributed by island arcs [*Allègre et al*., 2010], which are driven by crust subduction. We therefore assume that island basalt area (arc and ocean island) scales with the global material subduction rate, which has been estimated for 230 Ma to present [*Van Der Meer et al*., 2014]. We assume a constant rate before 230 Ma in the absence of data.

The individual LIP decay curves, island basalt area scaling, and resulting global basalt areas are shown in Figure 5. To account for difficulty in initial area estimation and incomplete preservation, we assume an

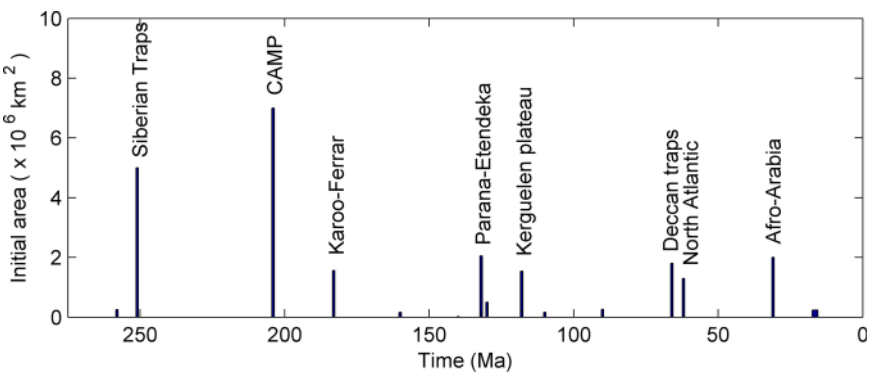

Figure 4. Initial subaerial areas of large igneous provinces. From an updated version of the Large Igneous Provinces Commission A10 database [*Ernst and Buchan*, 2001; *Ernst*, 2014] (see supporting information). Note the inclusion of the Kerguelen plateau, which is not a continental flood basalt, but was initially exposed above sea level [*Coffin et al*., 2000; *Mohr et al*., 2002].

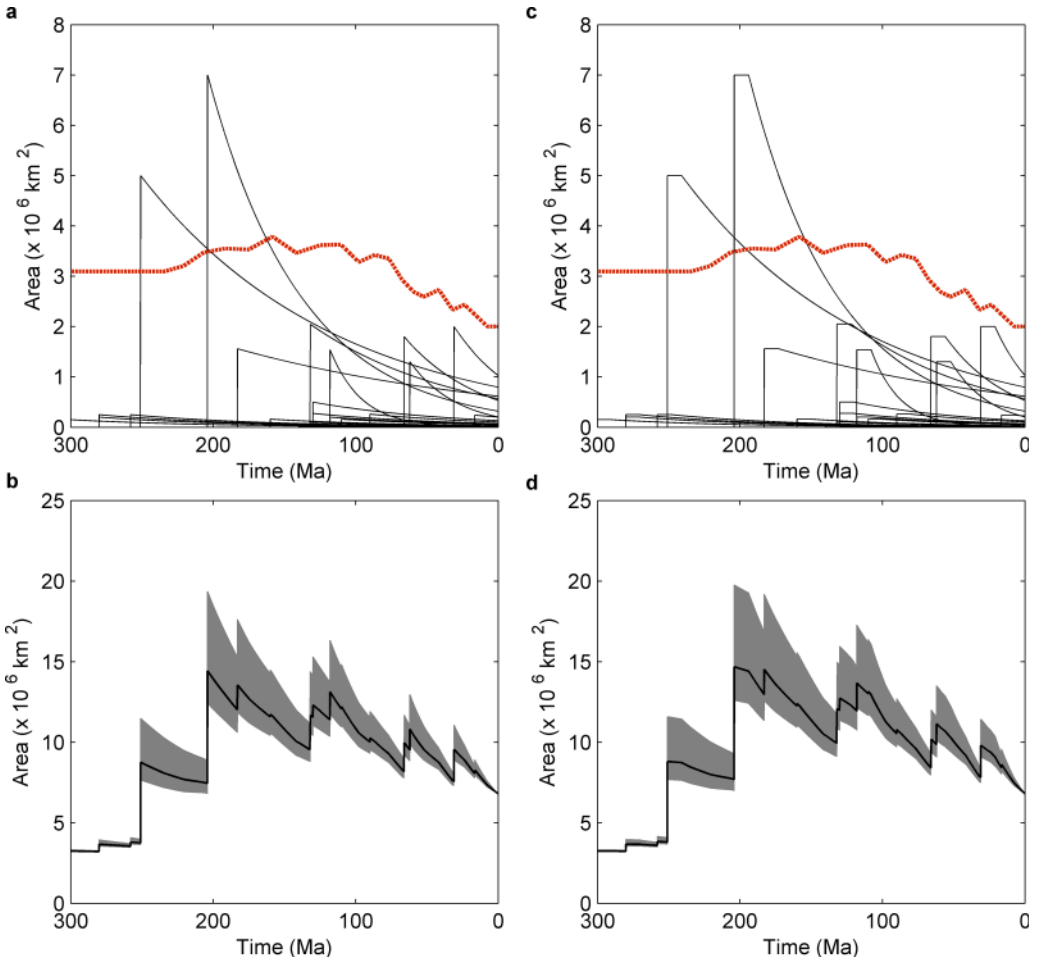

Figure 5. Reconstructed total basalt area for 300 Ma to present. Black decay curves show individual LIP areas, red dashed lines show total island basalt area (ocean islands and island arcs, assumed proportional to ocean crust destruction rate). Gray areas show resulting reconstruction for total basalt area, between 80% and 150% of the initial LIP areas shown in Figure 4 and inclusion of ocean islands and arcs, black lines show the unmodified areas. (a) Exponential decay; (b) resulting total basalt area; (c) delayed exponential decay; (d) resulting basalt area.

uncertainty of −20% and +50% on initial LIP areas to construct the gray areas in Figures 5b and 5d. This uncertainty window is based on the range of area estimates for well-studied LIPs (e.g., CAMP) [*Ernst*, 2014; *Ernst et al*., 2005; *Marzoli*, 1999], and incorporates the tendency for areas to be revised upward over time. Irrespective of the assumed LIP area and decay curves, the key features of the basalt area reconstruction are a peak after emplacement of the Central Atlantic Magmatic Province around 200 Ma, and a general decline from 200 Ma to present, with a two-stage decline throughout the Cenozoic. The "sawtooth" pattern is a result of the geologically rapid emplacement of LIPs, and the assumed rapid initial decline in area as the weatherable surface is removed. The ∼2–3-fold reduction in area between 200 Ma and present is due to the smaller area of more recent LIPs, and a declining rate of material subduction (driving arc basalt production).

The new reconstruction suggests that the global basaltic area was generally larger than the present day during the Jurassic and Cretaceous, due to a series of very large basaltic emplacements that accompanied the breakup phases of Pangaea. Highest values roughly coincide with the start of breakup (∼175 Ma) and subsequent smaller peaks are relatable to the later phases of breakup at ∼140 and ∼60 Ma.

A weakness of this approach for calculating basaltic area is the assumption of a constant decay regime over time. It is more likely that decay rates were greatly affected by paleogeographic position and therefore local climate. We believe that this method represents a reasonable first attempt to document integrated basalt area over time from primary data, and expect this type of reconstruction to improve in future work, where

the use of spatial models [*Taylor et al*., 2012; *Lefebvre et al*., 2013] can simulate local weathering, erosion, and tectonic regimes—and thus more accurately simulate the removal rates of individual LIPs.

3.5. Modeling Seafloor Weathering

The expression for seafloor weathering follows a previous incorporation of this flux into COPSE [*Mills et al*., 2014], which is based on the model of *Sleep and Zahnle* [2001]. The CO_2 dependence of seafloor weathering follows *Brady and Gislason* [1997], assuming that bottom water temperature controls reaction rate. The rate is inferred here from atmospheric CO_2 [*Brady and Gislason*, 1997] rather than that of the deep water—as has been used by *Goddéris and Francois* [1995]. Other indirect feedbacks on CO_2 may exist [*Coogan and Gillis*, 2013] but require quantification.

$$sfw = k_{sfw} \cdot Sp_{rel} \cdot (RCO_2)^{\alpha}. \quad (11)$$

Here Sp_{rel} is the relative crustal generation (i.e., spreading) rate, RCO_2 denotes the relative concentration of CO_2 in the atmosphere and $k_{sfw} = 1.75 \times 10^{12}$ mol/yr is the assumed present-day rate, taken between current estimates [*Alt and Teagle*, 1999; *Gillis and Coogan*, 2011; *Staudigel et al*., 1989]. $\alpha = 0.23$ represents the power of the feedback strength of CO_2 on seafloor weathering [*Brady and Gislason*, 1997], $\alpha = 0$ (no feedback on CO_2) is also trialed. Ocean crust generation rate is assumed to follow the calculated degassing rate of *Van Der Meer et al*. [2014], following the assumption that plate creation and destruction rates are equivalent over long time scales. We note the limitations of this approximation and that both the present-day rate and the response to CO_2 concentration have large uncertainties attached (see supporting information Figure S1 for the effect of varying present-day rate on the model).

3.6. The Strontium Cycle and $^{87}Sr/^{86}Sr$

We add to COPSE a strontium isotope system based on the work of *Francois and Walker* [1992] and *Vollstaedt et al*. [2014]. Although we do not expect this model to reproduce the ocean $^{87}Sr/^{86}Sr$ record exactly due to the reservations listed previously, it may be possible to correlate certain features of the record with changes in terrestrial and seafloor weathering regimes. Ocean Sr sources are the weathering of terrestrial granites, basalts and carbonates, and mantle input. The $^{87}Sr/^{86}Sr$ values of silicates are fixed (with an added expression for increase due to Rb decay), whereas the values for carbonates are allowed to vary depending on buried material. Model Sr sinks are the incorporation of strontium in carbonate sediments and altered seafloor basalt. We stress that an arbitrary error envelope can be added to any model Sr curve due to heterogeneity in terrestrial rock ages, which is not considered here. For full details of the Sr cycle see the SI.

4. Model Results and Discussion

4.1. Metamorphic Degassing and Weathering

Figure 6 shows COPSE model output for relative atmospheric CO_2 concentration and ocean $^{87}Sr/^{86}Sr$ for 230–0 Ma when subject to the *Van Der Meer et al*. [2014] degassing rate. Figures 6a and 6b show results when seafloor weathering is assumed to not be impacted by changing CO_2 concentration ($\alpha = 0$), Figures 6c and 6d show results when the feedback strength is assumed to be that of the bottom water temperature mechanism only ($\alpha = 0.23$ [*Brady and Gislason*, 1997]). LIP degassing is not considered here.

Running the default COPSE model (no consideration of basalt or seafloor weathering) with the addition of the recent reconstruction for CO_2 degassing results in high CO_2 concentration for the entire timeframe (dashed gray lines) and shows a poor fit to available proxy data, except for the late Cenozoic [*Park and Royer*, 2011]. This is because the *Van Der Meer et al*. [2014] degassing reconstruction is significantly higher than the GEOCARB/COPSE reconstruction over much of the model timeframe.

Adding seafloor weathering brings model CO_2 predictions closer to proxy data (black dashed lines). This is because we assume seafloor weathering is enhanced when the mid-ocean production rate is higher, meaning that proposed high degassing rates over the Mesozoic may have been countered by an increase in carbon sequestration via seafloor weathering. Allowing seafloor weathering to also respond to changes in CO_2 ($\alpha = 0.23$; Figures 6c and 6d) results in stronger regulation and lower predicted CO_2 concentrations. Under the addition of basalt and seafloor weathering, predicted CO_2 concentration is further reduced and now reasonably in line with geologic estimates for $\alpha = 0.23$. The larger basalt area in the Mesozoic acts to increase global terrestrial weatherability, which leads to lower steady state CO_2 concentration.

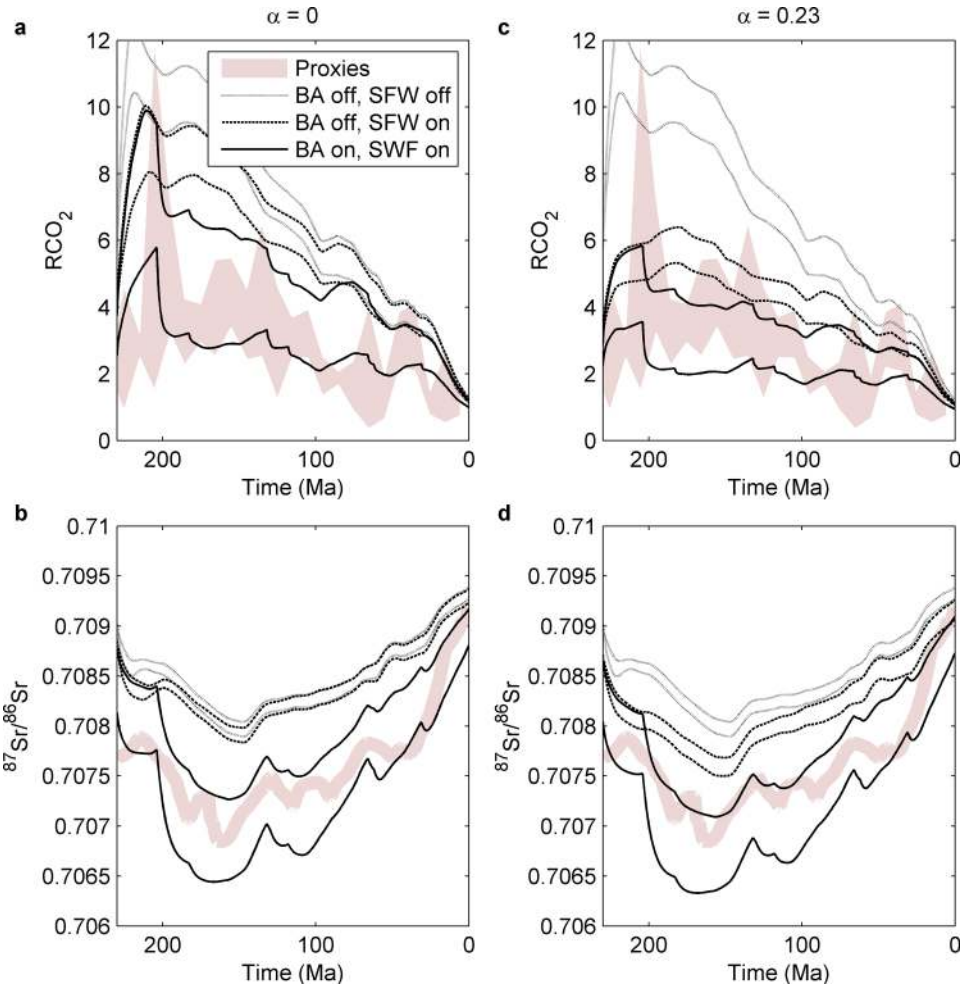

Figure 6. COPSE model output for 230–0 Ma when subject to basalt weathering and seafloor weathering. (a, c) Relative CO_2 concentration. (b, d) Predicted ocean $^{87}Sr^{86}Sr$. Gray dashed lines show COPSE model with updated degassing forcing [*Van Der Meer et al*., 2014] but without inclusion of basalt and seafloor weathering. Black dashed lines show inclusion of seafloor weathering only. The two lines represent the upper and lower bounds of the degassing data in *Van Der Meer et al*. [2014]. Black lines show model solution space under inclusion of seafloor weathering and combined basalt areas from Figure 5. Pink areas show data for CO_2 [*Park and Royer*, 2011] and ocean $^{87}Sr^{86}Sr$ [*McArthur et al*., 2001].

The choice of LIP decay curves and uncertainty on initial LIP areas does not cause large variation in CO_2 predictions—the majority of the variation comes from the uncertainty in the degassing rate. This is expected as these modifications do not lead to large changes in the overall basalt area forcing (Figure 5). When LIP area is increased, CO_2 predictions are lower, as would be expected under increased terrestrial weatherability. The largest changes to CO_2 predictions between the different model setups are during the Jurassic and Cretaceous, where there is assumed to be a large weatherable volcanic area, and a high global spreading rate. Decline in basaltic area over the Cenozoic causes a reduction in terrestrial weatherability, which along with the decreasing seafloor spreading rate, brings predictions closer to the unforced model. CO_2 predictions for 100–75 Ma do not fit well with proxy data for any scenario, indicating either an error in one of the model forcings or mechanisms, or perhaps in the proxy data.

It appears that to counter high degassing rates during the Mesozoic may require some feedback between seafloor weathering rate and CO_2 concentration. Assuming no relationship between seafloor weathering and CO_2, we must assume very large areas for LIPs and minimum estimates for degassing in order to match proxy data (Figure 6a). In the modification of GEOCARB by *Van Der Meer et al*. [2014], low CO_2 is achieved under the high Mesozoic degassing rate without the addition of seafloor weathering. This requires the

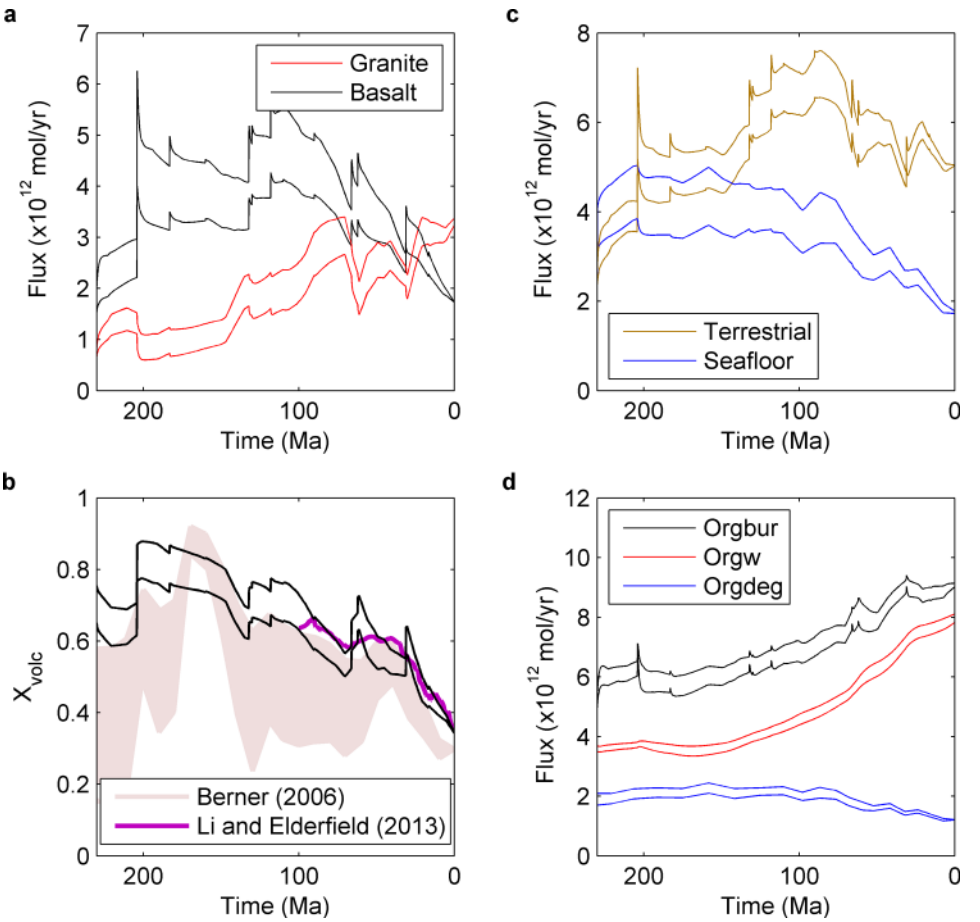

Figure 7. Weathering fluxes over model timeframe for $\alpha = 0.23$. (a) Terrestrial weathering of basalts (black) verses granites (red, assumed to make up the rest of terrestrial silicates). (b) Fraction of carbon flux from terrestrial silicate weathering that is the result of basalt weathering, compared to the same variable derived from isotope inversion models [*Berner*, 2006b; *Li and Elderfield*, 2013]. (c) Terrestrial silicate weathering (brown) versus seafloor weathering (blue). (d) Organic carbon fluxes for burial (black), weathering (red) and degassing (blue).

maximum basalt weathering forcing from GEOCARB (their scenario with $NV = 0$ corresponds to the very top of the X_{volc} distribution of *Berner* [2006b]).

The unforced COPSE model (gray dashed line, Figure 6) shows a very poor fit to ocean $^{87}Sr/^{86}Sr$ data, which is to be expected as the $^{87}Sr/^{86}Sr$ ratio of terrestrial rock is fixed at the average crustal value. The trend in this output therefore reflects the total terrestrial silicate weathering flux, and the gradually increasing $^{87}Sr/^{86}Sr$ values due to ^{87}Rb decay. Adding seafloor weathering improves the fit very slightly by removing some of the terrestrial source of radiogenic Sr, which has been shown previously [*Francois and Walker*, 1992]. Adding seafloor weathering and basalt weathering to the model results in improved prediction of the $^{87}Sr/^{86}Sr$ record; increased weathering of low-$^{87}Sr/^{86}Sr$ basalts over the Mesozoic lowers the curve significantly, and peaks followed by declining trends at ~200 Ma, ~130 Ma and ~65 Ma are reproduced to some extent—due to peaks in the basalt area forcing which result from emplacement of large igneous provinces at these times. The peaks in the Sr prediction correspond to decreasing basalt area before LIP emplacement events, poor replication of $^{87}Sr/^{86}Sr$ prior to 200 Ma may be related to the increased uncertainty on the areas of older LIPs.

As with any Sr isotope model, the results depend greatly on the assumed values for $^{87}Sr/^{86}Sr$ of carbonates. For all model runs we assume a starting value for carbonate $^{87}Sr/^{86}Sr$ of 0.714, which allows recovery of present-day ocean $^{87}Sr/^{86}Sr$ in the baseline model. $^{87}Sr/^{86}Sr$ of carbonates is a dynamic variable in the model, and reflects changes in the source and sink fractionations. Thus, over the model timeframe the $^{87}Sr/^{86}Sr$ of carbonates decreases due to burial of unradiogenic material to ~0.7075 at the present day, which is close to current values for carbonate weathering (0.7077) [*Li et al.*, 2009]. However, our reasonably

successful reproduction of ocean $^{87}Sr/^{86}Sr$ represents only one way of achieving this. Assuming different starting values and changes in carbonate $^{87}Sr/^{86}Sr$ (i.e., due to heterogeneous weathering of rocks of differing ages) could lead to accurate prediction of ocean $^{87}Sr/^{86}Sr$ under different tectonic and weathering regimes.

Our method does however show that the weathering regimes predicted by the model are not falsified by strontium data, and we believe it also provides an encouraging hypothesis for changes in Mesozoic-Cenozoic $^{87}Sr/^{86}Sr$. *Van Der Meer et al.* [2014] have shown that the general long-term trend in the $^{87}Sr/^{86}Sr$ curve may be related to weathering of volcanic rocks and mantle inputs associated with their degassing reconstruction, we add to this that the finer-scale details may be attributed to the emplacement of large igneous provinces. Even so, our model fails to completely capture the rapidity of the $^{87}Sr/^{86}Sr$ rise over the last 40 Myrs. This may be attributed to extremely radiogenic Sr sources from Himalayan rivers [*Galy et al.*, 1999], which exceed our assumed $^{87}Sr/^{86}Sr$ of "granitic" rocks, or to a more rapid uplift effect than is used in the model. However, model integrations under the more rapid Cenozoic uplift reconstruction of *Hay et al.* [2006] do not show an improved fit to strontium or CO_2 data (see supporting information Figure S2).

Figure 7 shows the shifts between basalt, granite, and seafloor weathering regimes as predicted by the forward model. Results imply that that basalt was the greater contributor to total terrestrial silicate weathering during the Triassic, Jurassic, and Cretaceous. During the Cenozoic, basalt weathering decreases significantly while granite weathering increases somewhat, becoming the greater flux in the last ~20 Myr. Total terrestrial silicate weathering peaks around 100 Ma, driven by a very large basalt weathering flux at this time.

Comparing the model output for the volcanic fraction (i.e., basalt fraction) of terrestrial silicate weathering (X_{volc}; Figure 7b) to the same parameter calculated from isotope inverse modeling by *Berner* [2006b] shows that we are at the upper end of Berner's estimates over the model timeframe. A key point of agreement is the middle to late Jurassic (~175–150 Ma), where Berner's isotope inversion requires around 80–90% of silicate weathering to come from basalts in order to match the extremely low $^{87}Sr/^{86}Sr$ values for this time. Our model replicates the minimum in $^{87}Sr/^{86}Sr$ at this time under $X_{volc} \approx 0.8$. Our predictions of X_{volc} agree well over the past 100 Myr with the inverse model inferences of *Li and Elderfield* [2013].

This work, Berner's isotope inversion, and the multiple-isotope-inversion model of *Li and Elderfield* [2013] all predict a reduction in the volcanic fraction of terrestrial silicate weathering over the Cenozoic. Our model can assign a definite cause for this—the decrease in basalt area due to falling rate of high-area LIP emplacement and falling subduction rates (driving arc volcanism). The decrease in Cenozoic X_{volc} in our model is comparable to these other approaches, consistent with a reasonable reproduction of the rise in $^{87}Sr/^{86}Sr$.

Figure 7c compares weathering fluxes from total terrestrial silicates (all basalt + granite) with seafloor weathering. The two fluxes generally follow the same pattern, which is expected as they both are dependent on atmospheric CO_2 concentration. However, the fluxes begin to diverge around 150 Ma, meaning that for 230–150 Ma seafloor weathering is similarly important as terrestrial silicate weathering in the carbon cycle, and for 150–0 Ma the terrestrial flux gradually becomes much more important. This shift is due to enhancement of terrestrial weathering fluxes in COPSE-driven by increasing uplift rates and the evolution of angiosperms on the land surface, and also driven by decreasing rates of ocean ridge production—which weaken the seafloor weathering sink. These factors combine to shift the balance of CO_2 sinks away from seafloor alteration and toward terrestrial silicate weathering [*Mills et al.*, 2014].

This supports the hypothesis, based on a fivefold decrease in calcite concentrations in the upper oceanic crust, that seafloor weathering was a stronger climate regulator during the Mesozoic, and had a less important role in the Cenozoic [*Coogan and Gillis*, 2013], although determining the source of calcite in seafloor basalts still poses a problem. It also makes the suggestion that this switch was driven by a combination of tectonic and biotic processes.

Figure 7d shows the model organic carbon fluxes, which are largely controlled by erosion rates, and thus follow the uplift forcing, aside from organic carbon degassing at subduction zones, which scales with the degassing forcing. Rapid emplacement of LIPs is predicted to drive spikes in organic carbon burial due to additional nutrient delivery from fresh basaltic terrains.

In Figure 8, we revisit the degassing scenario used in the original GEOCARB and COPSE models (see Figure 1). The degassing curve is similar to the estimations of *Van Der Meer et al.* [2014] for 100–0 Ma but the GEOCARB approximation has much lower values, close to the present day, for 230–100 Ma. As would be

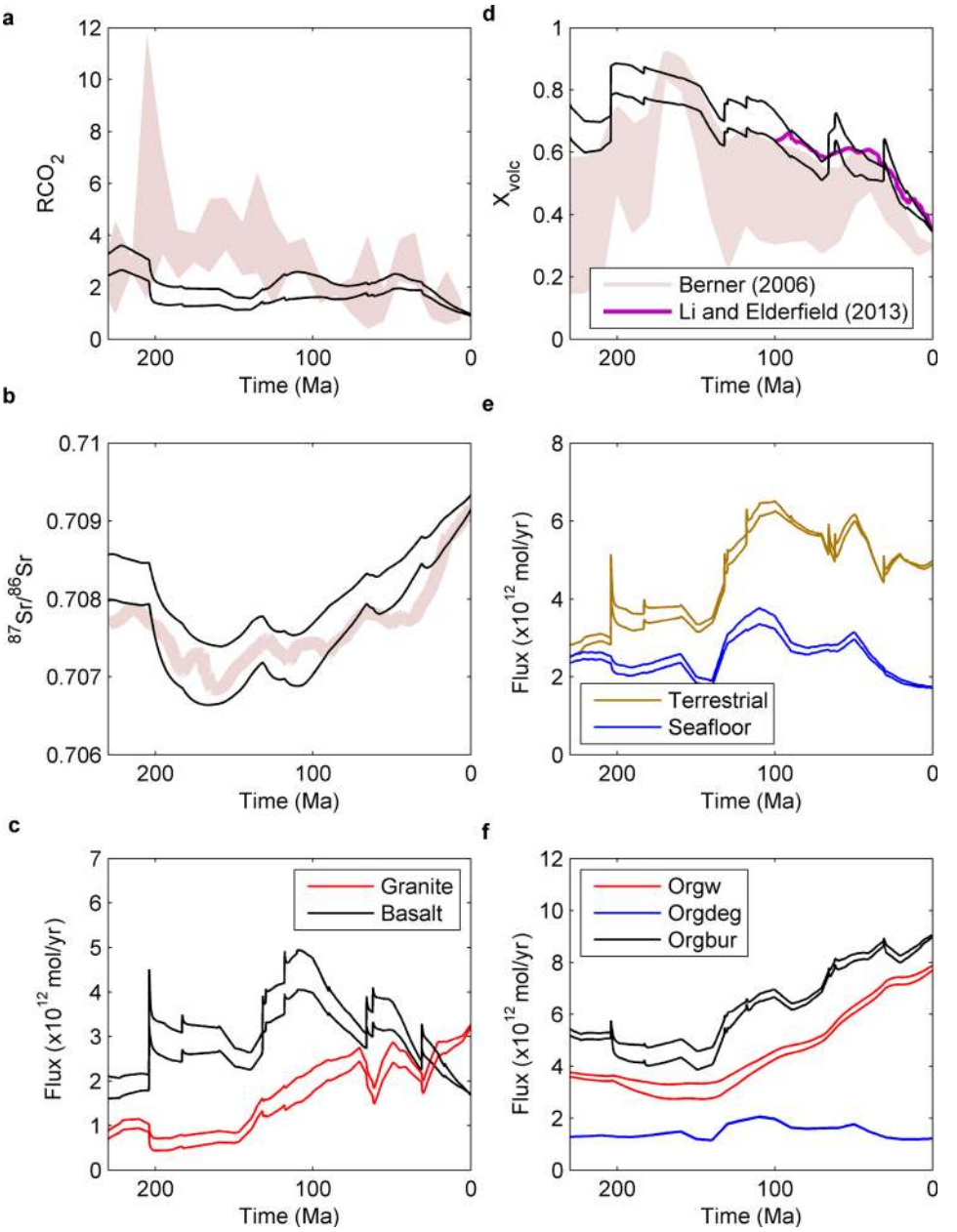

Figure 8. COPSE model output for 230–0 Ma when subject to basalt weathering and seafloor weathering ($\alpha = 0.23$), under original GEOCARB degassing scenario (see Figure 1). (a) Relative CO_2 concentration. (b) Predicted ocean $^{87}Sr^{86}Sr$. (c) Weathering of basalts (black) and granites (red). (d) Fraction of carbon flux from terrestrial silicate weathering that is the result of basalt weathering, compared to the same variable derived from isotope inversion models [*Berner*, 2006b; *Li and Elderfield*, 2013]. (e) Terrestrial silicate weathering (brown) versus seafloor weathering (blue). (f) Organic carbon fluxes for burial (black), weathering (red) and degassing (blue). Areas show model solution space under inclusion of CO_2 degassing scenarios, seafloor weathering and total basalt areas from Figure 5. Pink areas show data for CO_2 [*Park and Royer*, 2011] and ocean $^{87}Sr^{86}Sr$ [*McArthur et al.*, 2001].

expected, modeled CO_2 concentrations for 230–100 Ma are now considerably lower than proxy estimates. Under GEOCARB degassing, seafloor weathering remains smaller than terrestrial silicate weathering for the whole model timeframe, and does not show significant step change between the Mesozoic and present day. Granite and basalt weathering fluxes are also lowered for 230–100 Ma, as is required to balance the carbon cycle, but the volcanic fraction of weathering (X_{volc}) remains similar.

Our modeling lends support to the degassing reconstruction of *Van Der Meer et al.* [2014], reasoning that the large area of weatherable basalts expected during the early and mid-Mesozoic would imply much lower

CO_2 than suggested by proxies [*Park and Royer*, 2011], unless countered by higher degassing rates. Low Mesozoic degassing would have to be accompanied by much smaller basalt and seafloor weathering fluxes in order to reproduce CO_2 proxies, which has been assumed in previous models, but we question here.

Although our modeling can reproduced CO_2 proxies reasonably, many features of the proxy record are not reproduced, such as high early Cenozoic CO_2. It may be that using spatial paleogeographic reconstructions will allow models to match these data, or there may be further important mechanisms that are missing from current models.

4.2. CO_2 Input and Seafloor Weathering Due to LIP Emplacement

Figure 9 shows model predictions for CO_2 and $^{87}Sr/^{86}Sr$ when subject to LIP CO_2 degassing alongside the forcing factors in Figure 6 ($\alpha = 0.23$ case). This scenario assumes the *Van Der Meer et al.* [2014] global degassing curve and that each LIP degasses over 200 kyr. The result is a series of spikes in CO_2 concentration, which cause small positive "humps" in $^{87}Sr/^{86}Sr$ due to increased terrestrial weathering as a result of rising temperature. Assuming the minimum amount of CO_2 per km^3 of basalt, the degassing does not significantly alter model predictions. Taking a maximum assumption here results in clear CO_2 spikes, with the atmosphere and ocean CO_2 inventory almost doubling during eruption of the Ontong-Java plateau. Other LIPs result in fairly modest long-term CO_2 rises, even when taking a maximum estimate for the CO_2-volume relationship.

The CAMP emplacement results in only a minor increase in atmospheric CO_2 concentration in our model, in contrast to the ~50% increase shown in the similar carbon cycle model of *Beerling and Berner* [2002] (the model run in question assumes ~13,000GtC emissions, roughly equal to our maximum of 10^{18} mol C). The difference can be accounted for by our consideration of the weathering of CAMP basalts, which partially nullify the CO_2 rise by increasing global weatherability, eventually bringing CO_2 to a steady state lower than the pre-CAMP value. Additionally, COPSE includes negative feedback on CO_2 via a nutrient-driven biosphere, which responds to enhanced weathering by burying more organic carbon (Figure 9f). Our assumption of higher background degassing (and therefore weathering) rates for the Mesozoic also reduces the effectiveness of adding more CO_2 (i.e., the fractional increase in CO_2 input is less). We therefore propose that unless injection is geologically very rapid ($<10^5$ years), the long term effects of CO_2 emissions from continental flood basalts may be substantially reduced by the associated highly weatherable rock areas that are emplaced. This work however does not consider potential climate drivers from mass extinctions and short term carbonate system feedbacks, which may have a substantial effect over shorter time scales. We also do not consider the changing proportion of ocean/atmosphere carbon that is contained in the atmosphere, which may be boosted by rapid injection before equilibrium is reached.

Submarine LIPs are assumed to influence seafloor weathering rates via increasing crustal production rates, which leads to damping of the associated CO_2 spikes. In the 200 kyr degassing scenarios shown, seafloor weathering rates are increased dramatically during the emplacement of Cretaceous ocean plateaux, and by an order of magnitude during the Ontong-Java emplacement (125 Ma). Assuming the minimum CO_2 degassing for the Ontong-Java leads to brief CO_2 decrease in the model, as enhancement of seafloor weathering outweighs the CO_2 source. Our approach here is preliminary, but may help to reconcile apparent falling Cretaceous CO_2 concentrations with such large CO_2 injection events. It should be noted that short term CO_2 variations resulting from oceanic LIP emplacements require much more detailed study, and an improved understanding of hydrothermal circulation within and around ocean plateaus to properly quantify their contribution to seafloor weathering.

Degassing times for LIPs may be significantly longer than 200 kyrs. Model runs under longer (typically 0.5–3 Myr) emplacement times, as compiled by *Courtilliot and Renne* [2003], show a reduction in the magnitude of CO_2 spikes, and seafloor weathering enhancements (supporting information Figure S3). Although the Ontong-Java plateau still causes a significant perturbation.

5. Summary and Conclusions

Our forward model reproduces Mesozoic and Cenozoic CO_2 concentrations satisfactorily, and correctly predicts many of the aspects of ocean $^{87}Sr/^{86}Sr$. It appears that recently-inferred high degassing rates during the Mesozoic [*Van Der Meer et al.*, 2014], if correct, would have been countered by increased rates of both

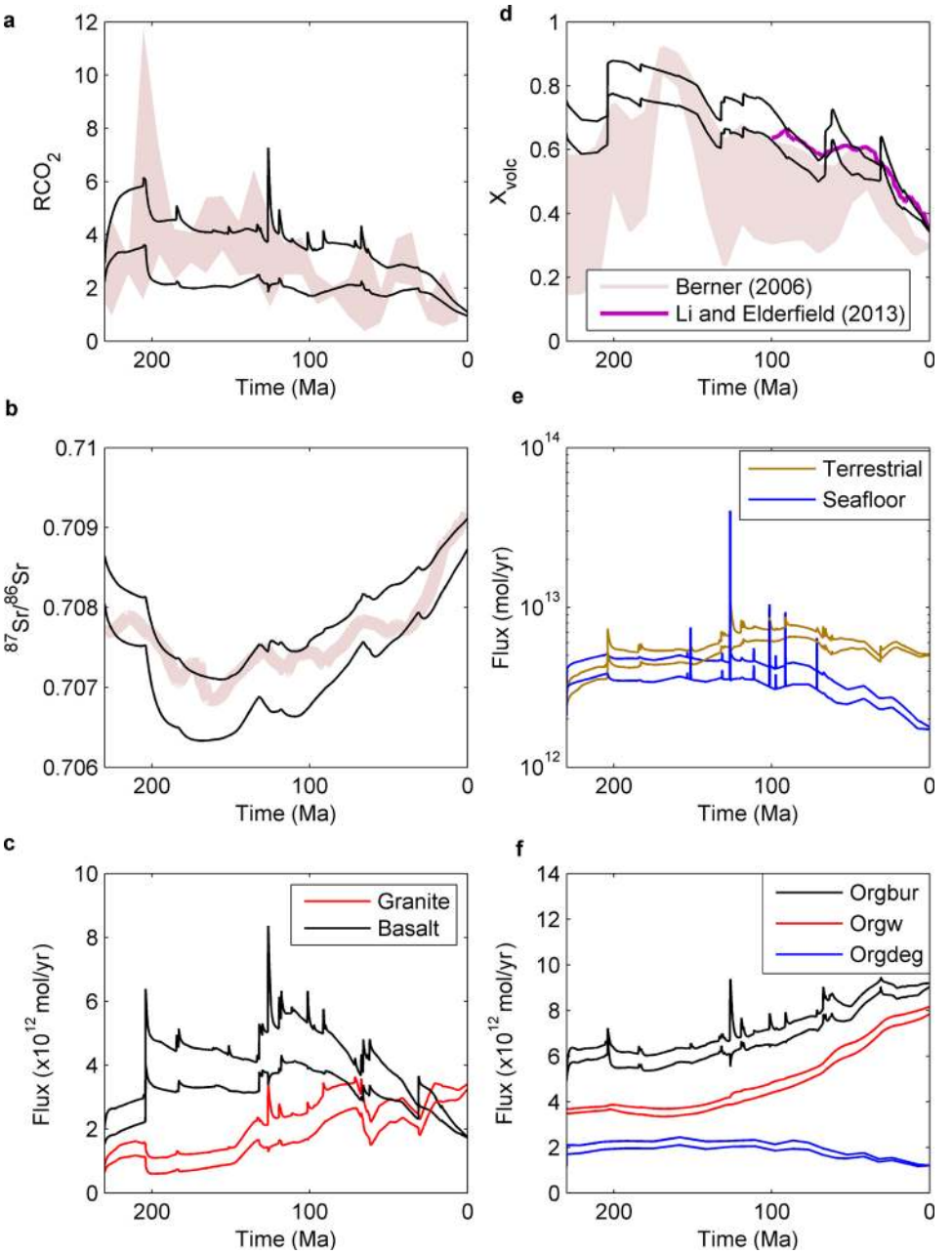

Figure 9. COPSE model output for 230–0 Ma when subject to basalt weathering and seafloor weathering ($\alpha = 0.23$), with LIP CO_2 releases over 200 kyr, and seafloor weathering rate dependent on LIP crustal generation. (a) Relative CO_2 concentration. (b) Predicted ocean $^{87}Sr^{86}Sr$. (c) Weathering of basalts (black) and granites (red). (d) Fraction of carbon flux from terrestrial silicate weathering that is the result of basalt weathering, compared to the same variable derived from isotope inversion models [*Berner*, 2006b; *Li and Elderfield*, 2013]. (e) Terrestrial silicate weathering (brown) versus seafloor weathering (blue). (f) Organic carbon fluxes for burial (black), weathering (red) and degassing (blue). Areas show model solution space under inclusion of CO_2 degassing scenarios, seafloor weathering and all terrestrial basalt areas from Figure 5. Pink areas show data for CO_2 [*Park and Royer*, 2011] and ocean $^{87}Sr^{86}Sr$ [*McArthur et al.*, 2001].

seafloor weathering and basalt weathering over this era, and not by basalt weathering alone. Consideration of the paleolatitude of LIPs and local hydrological regimes in future models could result in $^{87}Sr/^{86}Sr$ predictions falling even closer to the geologic record. While our model does include an increase in uplift during the Cenozoic [*Raymo and Ruddiman*, 1992], this is not the dominant factor driving Cenozoic CO_2 drawdown or the modeled rise in $^{87}Sr/^{86}Sr$. Instead, the drop in CO_2 is dominated by declining degassing (see supporting information Figure S4 for a model run with constant degassing) and the rise in $^{87}Sr/^{86}Sr$ is dominated by decreasing area of basalts undergoing weathering (Figure 6).

Our model defines three climate modes: Pre-Cretaceous CO_2 regulation is split almost equally between seafloor and terrestrial weathering, with basalt weathering exceeding granite weathering. During the Cretaceous, regulation begins to rely more heavily on terrestrial weathering, with basalt weathering still exceeding granite weathering, and Cenozoic regulation is still primarily terrestrial, but sees granites taking over from basalts. This distinction between weathering sources may be very important for the delivery of the limiting nutrient phosphate, and resulting oxygenation through organic carbon burial. Seafloor weathering does not result in P input [*Mills et al*., 2014] and phosphate availability differs between granites and basalts [*Porder and Ramachandran*, 2013]. Our results are dependent on the assumed CO_2 degassing curve: predictions for Mesozoic CO_2 concentration appear to support high degassing during this time [*Van Der Meer et al*., 2014]; however, the notion of a definitive reconstruction of degassing rates is far from resolved.

We have reconstructed the global basaltic area from primary data and simple decay relationships. Modeled basalt weathering under this constraint agrees well with the trends derived from isotope inversion methods [*Berner*, 2006b; *Li and Elderfield*, 2013]. The shift from basalt to nonbasalt weathering during the Cenozoic has been attributed to Himalayan uplift enhancing the nonbasalt flux [*Li and Elderfield*, 2013]. Here we conclude that a ~50% reduction in basaltic area during the Cenozoic was a key factor in reducing the silicate weathering flux from basalts over this time. The increased proportional weathering of granites over the Cenozoic in our model is a response to decreased basalt weathering, as well as uplift of granites—thus the "seesaw" carbon cycle of the Cenozoic [*Li and Elderfield*, 2013] may be controlled by either basalt or granite weathering enhancements.

Including additional isotope systems will enable these scenarios to be further tested. The Cenozoic lithium isotope record [*Misra and Froelich*, 2012] shows a rise in δ^7Li of ~9‰. This suggests [*Misra and Froelich*, 2012; *Froelich and Misra*, 2014] a change in terrestrial weathering regime from a supply limited Paleocene to a less-intense, kinetically limited present day, combined with a shift in seafloor sinks with an increase in removal by reverse-weathering (removal into sedimentary clays) relative to altered basalt [*Li and West*, 2014]. This is broadly consistent with our model results (with a decrease in temperature and increase in erosion over the Cenozoic). The model here also suggests additional factors that may contribute: the shift from basalt (with lower incongruent weathering [*Misra and Froelich*, 2012]) to granite weathering, and a decline in degassing (reducing both terrestrial silicate weathering intensity and low-temperature seafloor basalt alteration).

Long term CO_2 release from continental LIPs is countered in our model by the weathering effects of the newly emplaced basaltic area, as has been established by individual studies of these events [*Dessert et al*., 2001; *Grard et al*., 2005]. Large increases in CO_2 concentration associated with LIPs require geologically rapid CO_2 injection, or rely on shorter-term processes such as emissions from intrusion into organic materials and destabilization of methane hydrates [e.g., *Beerling and Berner*, 2002]. Similarly, CO_2 input from oceanic LIPs may be countered by increased seafloor basalt alteration.

The breakup phases of Pangaea are times of enhanced CO_2 degassing, but also seem to correlate with high proportions of weatherable volcanic area and enhancements of seafloor weathering. This seems plausible given that both LIP emplacements and continental breakup may be driven to some extent by mantle plumes and enhanced crustal production.

Recent spatial simulations of LIP locations for several time points during the Cenozoic [*Lefebvre et al*., 2013] suggest that weathering of igneous provinces may have generally increased over this time as LIPs encounter different regional climates. This trend appears contrary to the results shown here (see supporting information Figure S4 for a comparison), and does not show the decrease which we attribute to decay of LIP areas. Future work must focus on incorporating both local climatic changes [*Lefebvre et al*., 2013; *Kent and Muttoni*, 2013] and reconstructions of previous basalt areas into a dynamic model, in order to more accurately represent changing tectonic drivers of climate.

Acknowledgments
The authors thank John McArthur for the LOWESS $^{87}Sr/^{86}Sr$ data set and Gaojun Li for model output tables. B.M. is supported by the UK Natural Environment Research Council (NE/G018332/2). S.J.D. and T.M.L. are supported by the Leverhulme Trust (RPG-2013-106). T.M.L. is also supported by a Royal Society Wolfson Research Merit Award.

References

Allègre, C. J., P. Louvat, J. Gaillardet, L. Meynadier, S. Rad, and F. Capmas (2010), The fundamental role of island arc weathering in the oceanic Sr isotope budget, *Earth Planet. Sci. Lett.*, *292*, 51–56.

Alt, J. C., and D. A. H. Teagle (1999), The uptake of carbon during alteration of oceanic crust, *Geochim. Cosmochim. Acta*, *63*, 1527–1535.

Arvidson, R. S., F. T. Mackenzie, and M. Guidry (2006), MAGic: A Phanerozoic model for the geochemical cycling of major rock-forming components, *Am. J. Sci.*, *306*, 135–190.

Beerling, D. J., and R. A. Berner (2002), Biogeochemical constraints on the Triassic-Jurassic boundary carbon cycle event, *Global Biogeochem. Cycles*, *16*(3), 1036, doi:10.1029/2001GB001637.
Belcher, C. M., and L. Mander (2012), Catastrophe: Extraterrestrial impacts, massive volcanism, and the biosphere, in *The Future of the World's Climate*, edited by A. Henderson-Sellers and K. McGruffie, pp. 463–485, Elsevier, Amsterdam.
Bergman, N. M., T. M. Lenton, and A. J. Watson (2004), COPSE: A new model of biogeochemical cycling over Phanerozoic time, *Am. J. Sci.*, *304*, 397–437.
Berner, R. A. (1991), A model for atmospheric CO_2 over Phanerozoic time, *Am. J. Sci.*, *291*, 339–376.
Berner, R. A. (1994), Geocarb II: A revised model of atmospheric CO_2 over Phanerozoic time, *Am. J. Sci.*, *294*, 56–91.
Berner, R. A. (1997), The rise of plants and their effect on weathering and atmospheric CO_2, *Science*, *276*, 544–546.
Berner, R. A. (2002), Examination of hypotheses for the Permo-Triassic boundary extinction by carbon cycle modeling, *Proc. Natl. Acad. Sci. U. S. A.*, *99*(7), 4172–4177.
Berner, R. A. (2004), *The Phanerozoic Carbon Cycle: CO_2 and O_2*, Oxford Univ. Press, N. Y.
Berner, R. A. (2006a), GEOCARBSULF: A combined model for Phanerozoic atmospheric O_2 and CO_2, *Geochim. Cosmochim. Acta*, *70*, 5653–5664.
Berner, R. A. (2006b), Inclusion of the weathering of volcanic rocks in the GEOCARBSULF model, *Am. J. Sci.*, *306*, 295–302.
Berner, R. A., and Z. Kothavala (2001), Geocarb III: A revised model of atmospheric CO_2 over Phanerozoic time, *Am. J. Sci.*, *301*, 182–204.
Bluth, G. J. S., and L. R. Kump (1991), Phanerozoic paleogeology, *Am. J. Sci.*, *291*, 284–308.
Boucot, A. J., and J. Gray (2001), A critique of Phanerozoic climatic models involving changes in the CO content of the atmosphere, *Earth Sci. Rev.*, *56*, 1–159.
Brady, P. V., and S. R. Gislason (1997), Seafloor weathering controls on atmospheric CO_2 and global cimate, *Geochim. Cosmochim. Acta*, *61*, 965–973.
Bryan, S. E., and R. E. Ernst (2008), Revised definition of large igneous provinces (LIPs), *Earth Sci. Rev.*, *86*(1–4), 175–202.
Caldeira, K. (1995), Long-term control of atmospheric carbon dioxide: Low temperature seafloor alteration or terrestrial silicate rock weathering, *Am. J. Sci.*, *295*, 1077–1114.
Coffin, M., F. Frey, and P. Wallace (2000), Development of an intraoceanic large igneous province: The Kerguelen Plateau and Broken Ridge, Southern Indian Ocean, *JOIDES*, *26*, 5–9.
Coffin, M. F., and O. Eldholm (1994), Large igneous provinces: Crustal structure, dimensions, and external consequences, *Rev. Geophys.*, *32*, 1–36.
Coogan, L. A., and K. M. Gillis (2013), Evidence that low-temperature oceanic hydrothermal systems play an important role in the silicate-carbonate weathering cycle and long-term climate regulation, *Geochem. Geophys. Geosyst.*, *14*, 1771–1786, doi:10.1002/ggge.20113.
Courtilliot, V. E., and P. R. Renne (2003), On the ages of flood basalt events, *C. R. Geosci.*, *335*, 113–140.
Dessert, C., et al. (2001), Erosion of Deccan Traps determined by river geochemistry: Impact of the global climate and the $^{87}Sr/^{86}Sr$ ratio of seawater, *Earth Planet. Sci. Lett.*, *188*, 459–474.
Dessert, C., B. Dupre, J. Gaillardet, L. M. Francois, and C. J. Allegre (2003), Basalt weathering laws and the impact of basalt weathering on the global carbon cycle, *Chem. Geol.*, *202*, 257–273.
Dixon, J. L., A. S. Hartshorn, A. M. Heimsath, R. A. DiBiase, and K. X. Whipple (2012), Chemical weathering response to tectonic forcing: A soils perspective from the San Gabriel Mountains, California, *Earth Planet. Sci. Lett.*, *323–324*, 40–49.
Dupre, B., et al. (2003), Rivers, chemical weathering and Earth's climate, *C. R. Geosci.*, *335*, 1141–1160.
Engbretson, D. C., K. P. Kelley, H. J. Cashman, and M. A. Richards (1992), 180 million years of subduction, *GSA Today*, *2*, 93–100.
Ernst, R. E. (2014), *Large Igneous Provinces*, Cambridge Univ. Press, Cambridge, U. K.
Ernst, R. E., and K. L. Buchan (2001), Large mafic magmatic events through time and links to mantle plume-heads, *Geol. Soc. Am. Spec. Pap.*, *352*, 483–575.
Ernst, R. E., K. L. Buchan, and I. H. Campbell (2005), Frontiers in large igneous province research, *Lithos*, *79*, 271–297.
Francois, L. M., and J. C. G. Walker (1992), Modelling the Phanerozoic carbon cycle and climate: Constraints from the $^{87}Sr/^{86}Sr$ isotopic ratio of seawater, *Am. J. Sci.*, *292*, 81–135.
Froelich, F., and S. Misra (2014), Was the late Paleocene-early Eocene hot because the Earth was flat? An ocean lithium isotope view of mountain building, continental weathering, carbon dioxide, and Earth's Cenozoic climate, *Oceanography*, *27*, 36–49.
Gaffin, S. (1987), Ridge volume dependence on seafloor generation rate and inversion using long term sealevel change, *Am. J. Sci.*, *287*, 596–611.
Galy, A., C. France-Lanord, and L. Derry (1999), The strontium isotope budget of Himalayan Rivers in Nepal and Bangladesh, *Geochim. Cosmochim. Acta*, *63*, 1905–1025.
Gannoun, A., K. W. Burton, N. Vigier, S. R. Gíslason, N. Rogers, F. Mokadem, and B. Sigfússon (2006), The influence of weathering process on riverine osmium isotopes in a basaltic terrain, *Earth Planet. Sci. Lett.*, *243*(3–4), 732–748.
Gerlach, T. M., and E. J. Graeber (1985), Volatile budget of Kilauea volcano, *Nature*, *313*, 273–277.
Gillis, K. M., and L. A. Coogan (2011), Secular variation in carbon uptake into the ocean crust, *Earth Planet. Sci. Lett.*, *302*, 385–392.
Goddéris, Y., and L. M. Francois (1995), The Cenozoic evolution of the strontium and carbon cycles: Relative importance of continental erosion and mantle exchanges, *Chem. Geol.*, *126*, 169–190.
Goddéris, Y., Y. Donnadieu, G. Le Hir, V. Lefebvre, and E. Nardin (2014), The role of palaeogeography in the Phanerozoic history of atmospheric CO_2 and climate, *Earth Sci. Rev.*, *128*, 122–138.
Grard, A., L. M. Francois, C. Dessert, B. Dupre, and Y. Godderis (2005), Basaltic volcanism and mass extinction at the Permo-Triassic boundary: Environmental impact and modeling of the global carbon cycle, *Earth Planet. Sci. Lett.*, *234*, 207–221.
Hay, W. W., et al. (2006), Evaporitves and the salinity of the ocean during the Phanerozoic: Implications for climate, ocean circulation and life, *Palaeogeogr. Palaeoclimatol. Palaeoecol.*, *240*, 3–46.
Hayes, J. M., and J. R. Waldbauer (2006), The carbon cycle and associated redox processes through time, *Philos. Trans. R. Soc. B*, *361*, 931–950.
Kent, D. V., and G. Muttoni (2013), Modulation of Late Cretaceous and Cenozoic climate by variable drawdown of atmospheric pCO_2 from weathering of basaltic provinces on continents drifting through the equatorial humid belt, *Clim. Past*, *9*, 525–546.
Knight, K. B., S. Nomade, P. R. Renne, A. Marzoli, H. Bertrand, and N. Youbi (2004), The Central Atlantic Magmatic Province at the Triassic–Jurassic boundary: Paleomagnetic and $^{40}Ar/^{39}Ar$ evidence from Morocco for brief, episodic volcanism, *Earth Planet. Sci. Lett.*, *228*, 143–160.
Kump, L. R., and M. A. Arthur (1997), Global chemical erosion during the Cenozoic: Weatherability balances the budgets, in *Tectonic Uplift and Climate Change*, edited by W. F. Ruddiman, pp. 399–426, Springer, N. Y.

Leavitt, S. W. (1982), Annual volcanic carbon dioxide emissions: An estimate from eruptions chronologies, *Environ. Geol.*, *4*, 15–21.
Lefebvre, V., Y. Donnadieu, Y. Godderis, F. Fluteau, and L. Hubert-Theou (2013), Was the Antarctic glaciation delayed by a high degassing rate during the early Cenozoic?, *Earth Planet. Sci. Lett.*, *371–372*, 203–211.
Lenton, T. M., and A. J. Watson (2000), Redfield revisited: II. What regulates the oxygen content of the atmosphere?, *Global Biogeochem. Cycles*, *14*, 249–268.
Li, G., and H. Elderfield (2013), Evolution of carbon cycle over the past 100 million years, *Geochim. Cosmochim. Acta*, *103*, 11–25.
Li, G., and A. J. West (2014), Evolution of Cenozoic seawater lithium isotopes: Coupling of global denudation regime and shifting seawater sinks, *Earth Planet. Sci. Lett.*, *401*, 284–293.
Li, G., J. Ji, J. Chen, and D. B. Kemp (2009), Evolution of the Cenozoic carbon cycle: The roles of tectonics and CO_2 fertilization, *Global Biogeochem. Cycles*, *23*, GB1009, doi:10.1029/2008GB003220.
Maher, K., and C. P. Chamberlain (2014), Hydrologic regulation of chemical weathering and the geologic carbon cycle, *Science*, *343*(6178), 1502–1504.
Marzoli, A. (1999), Extensive 200-million-year-old continental flood basalts of the Central Atlantic Magmatic Province, *Science*, *284*(5414), 616–618.
McArthur, J. M., R. J. Howarth, and T. R. Bailey (2001), Strontium isotope stratigraphy: LOWESS Version 3: Best fit to the marine Sr-isotope curve for 0–509 Ma and accompanying look-up table for deriving numerical age, *J. Geol.*, *109*, 155–170.
Mills, B., T. M. Lenton, and A. J. Watson (2014), Proterozoic oxygen rise linked to shifting balance between seafloor and terrestrial weathering, *Proc. Natl. Acad. Sci. U. S. A.*, *111*, 9073–9078.
Misra, S., and P. N. Froelich (2012), Lithium isotope history of Cenozoic Seawater: Changes in silicate weathering and reverse weathering, *Science*, *335*, 818–823.
Mohr, B. A. R., V. Wähnert, and D. Lazarus (2002), Mid-Cretaceous paleobotany and palynology of the Central Kerguelen Plateau, Southern Indian Ocean (ODP Leg 183, Site 1138), in *Proceedings of the Ocean Drilling Program, Scientific Results*, vol. 183, edited by F. A. Frey et al., pp. 1–39, Ocean Drill. Program, College Station, Tex.
Neal, C. R., J. J. Mahoney, L. W. Kroenke, R. A. Duncan, and M. G. Petterson (1997), The Ontong Java Plateau, in *Large Igneous Provinces—Continental, Oceanic, and Planetary Flood Volcanism, Geophys. Monogr. 100*, edited by J. J. Mahoney, pp. 183–215, AGU, Washington, D. C.
Park, J., and D. L. Royer (2011), Geologic constraints on the glacial amplification of Phanerozoic climate sensitivity, *Am. J. Sci.*, *311*, 1–26.
Peucker-Ehrenbrink, B., and J. D. Blum (1998), Re-Os isotope systematics and weathering of Precambrian crustal rocks: Implications for the marine osmium isotope record, *Geochim. Cosmochim. Acta*, *62*, 3193–3203.
Peucker-Ehrenbrink, B., and G. Ravizza (2012), Osmium isotope stratigraphy, in *The Geologic Time Scale 2012*, edited by F. M. Gradstein et al., pp. 45–165, Elsevier, Boston, USA.
Porder, S., and S. Ramachandran (2013), The phosphorus concentration of common rocks—A potential driver of ecosystem P status, *Plant Soil*, *367*, 41–55.
Raymo, M. E., and W. F. Ruddiman (1992), Tectonic forcing of late Cenozoic climate, *Nature*, *359*, 117–122.
Ronov, A. B. (1993), *Stratisfera—Ili Osadochnaya Obolochka Zemli (Kolichestvennoe Issledovanie)* [in Russian], edited by A. A. Yaroshevskii, 144 pp., Nauka, Moskva.
Sleep, N. H., and K. Zahnle (2001), Carbon dioxide cycling and implications for climate on ancient Earth, *J. Geophys. Res.*, *106*, 1373–1399.
Staudigel, H., S. R. Hart, H.-U. Schmincke, and B. M. Smith (1989), Cretaceous ocean crust at DSDP sites 417 and 418: Carbon uptake from weathering verses loss by magmatic outgassing, *Geochim. Cosmochim. Acta*, *53*, 3091–3094.
Svensen, H., S. Planke, A. G. Polozov, N. Schmidbauer, F. Corfu, Y. Y. Podladchikov, and B. Jamtveit (2009), Siberian gas venting and the end-Permian environmental crisis, *Earth Planet. Sci. Lett.*, *277*, 490–500.
Taylor, L. L., S. A. Banwart, P. J. Valdes, J. R. Leake, and D. J. Beerling (2012), Evaluating the effects of terrestrial ecosystems, climate and carbon dioxide on weathering over geological time: A global-scale process-based approach, *Philos. Trans. R. Soc. B*, *367*, 565–582.
Torres, M. A., A. J. West, and G. Li (2014), Sulphide oxidation and carbonate dissolution as a source of CO_2 over geological timescales, *Nature*, *507*, 346–349.
Van Der Meer, D. G., R. E. Zeebe, D. J. J. Hinsbergen, A. Sluijs, W. Spakman, and T. H. Torsvik (2014), Plate tectonic controls on atmospheric CO_2 levels since the Triassic, *Proc. Natl. Acad. Sci. U. S. A.*, *111*, 4380–4385.
Vollstaedt, H., et al. (2014), The Phanerozoic $\delta^{88/86}$Sr record of seawater: New constraints on past changes in oceanic carbonate fluxes, *Geochim. Cosmochim. Acta*, *128*, 249–265.
Walker, J. C. G., P. B. Hays, and J. F. Kasting (1981), A negative feedback mechanism for the long-term stabilization of Earth's surface temperature, *J. Geophys. Res.*, *86*, 9776–9782.
West, A. J. (2012), Thickness of the chemical weathering zone and implications for erosional and climatic drivers of weathering and for carbon-cycle feedbacks, *Geology*, *40*, 811–814.